HHS Public Access

Author manuscript

Org Lett. Author manuscript; available in PMC 2023 November 27.

Published in final edited form as:

Org Lett. 2022 December 30; 24(51): 9468–9472. doi:10.1021/acs.orglett.2c03922.

Photochemical Dimerization of Plakinidine B Leads to Potent Inhibition of the E3 Ubiquitin-Protein Ligase CBL-B

Quan T. Khong,
Molecular Targets Program, Center for Cancer Research, National Cancer Institute, Frederick, Maryland 21702-1201, United States

Donghao Li,
Chemical Biology Laboratory, Center for Cancer Research, National Cancer Institute, Frederick, Maryland 20850, United States

Brice A. P. Wilson,
Molecular Targets Program, Center for Cancer Research, National Cancer Institute, Frederick, Maryland 21702-1201, United States

Kalina Ranguelova,
Bruker BioSpin Corp, Billerica, Massachusetts 01821, United States

Masoumeh Dalilian,
Molecular Targets Program, Center for Cancer Research, National Cancer Institute, Frederick, Maryland 21702-1201, United States

Basic Science Program, Leidos Biomedical Research, Inc., Frederick National Laboratory for Cancer Research, Frederick, Maryland 21702-1201, United States

Emily A. Smith,
Molecular Targets Program, Center for Cancer Research, National Cancer Institute, Frederick, Maryland 21702-1201, United States

Basic Science Program, Leidos Biomedical Research, Inc., Frederick National Laboratory for Cancer Research, Frederick, Maryland 21702-1201, United States

Antony Wamiru,
Molecular Targets Program, Center for Cancer Research, National Cancer Institute, Frederick, Maryland 21702-1201, United States

Basic Science Program, Leidos Biomedical Research, Inc., Frederick National Laboratory for Cancer Research, Frederick, Maryland 21702-1201, United States

Ekaterina I. Goncharova,
Molecular Targets Program, Center for Cancer Research, National Cancer Institute, Frederick, Maryland 21702-1201, United States

Corresponding Authors dul2@mail.nih.gov, okeefeba@mail.nih.gov.

The authors declare no competing financial interest.

Complete contact information is available at: https://pubs.acs.org/10.1021/acs.orglett.2c03922

Advanced Biomedical Computational Science, Frederick National Laboratory for Cancer Research, Frederick, Maryland 21702-1201, United States

Tanja Grkovic,
Molecular Targets Program, Center for Cancer Research, National Cancer Institute, Frederick, Maryland 21702-1201, United States

Natural Products Branch, Developmental Therapeutics Program, Division of Cancer Treatment and Diagnosis, National Cancer Institute, Frederick, Maryland 21701-1201, United States

Donna Voeller,
Women's Malignancies Branch, Center for Cancer Research, National Cancer Institute, National Institutes of Health, Bethesda, Maryland 20892-1578, United States

Stanley Lipkowitz,
Women's Malignancies Branch, Center for Cancer Research, National Cancer Institute, National Institutes of Health, Bethesda, Maryland 20892-1578, United States

Martin J. Schnermann,
Chemical Biology Laboratory, Center for Cancer Research, National Cancer Institute, Frederick, Maryland 20850, United States

Barry R. O'Keefe,
Molecular Targets Program, Center for Cancer Research, National Cancer Institute, Frederick, Maryland 21702-1201, United States

Natural Products Branch, Developmental Therapeutics Program, Division of Cancer Treatment and Diagnosis, National Cancer Institute, Frederick, Maryland 21701-1201, United States

Lin Du
Molecular Targets Program, Center for Cancer Research, National Cancer Institute, Frederick, Maryland 21702-1201, United States

Abstract

A new dimeric alkaloid plakoramine A [(±)-**1**] was identified from a marine sponge *Plakortis* sp. Chiral-phase HPLC separation of (±)-**1** led to the purified enantiomers (+)-**1** and (−)-**1** which both potently inhibited CBL-B E3 ubiquitin ligase activities. The absolute configurations of the enantiomers were determined by quantum chemical calculations. Scrutinization of the purification conditions revealed a previously undescribed, nonenzymatic route to form (±)-**1** via photochemical conversion of its naturally occurring monomeric counterpart, plakinidine B (**2**).

Graphical Abstract

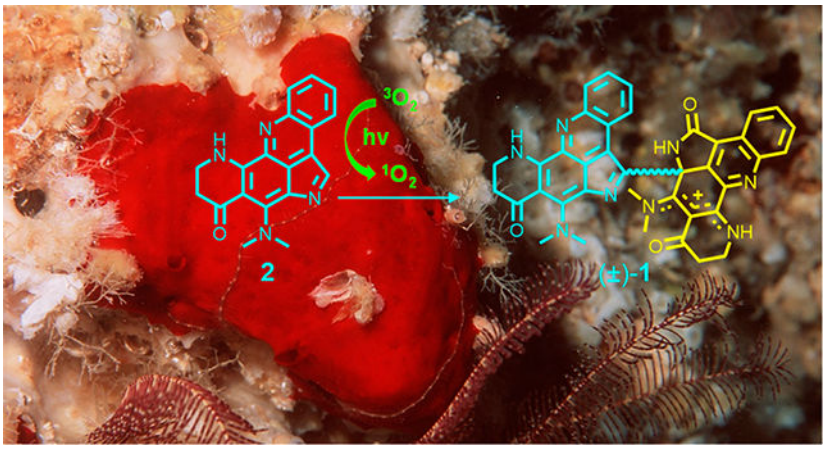

Dimerization is an energetically economical biosynthetic strategy that nature commonly adopts to generate complex natural product architectures.[1,2] In 2004, a survey on ca. 3000 articles estimated that about 15–20% of natural products were derivatized by a dimerization process.[3] The past decade has seen a significant increase in the study of dimeric natural products mainly arising from their potential therapeutical utility. A quick search of “dimeric natural products” as a keyword in SciFinder returned 849 publications from 2010 to date comparing to the total of only 561 publications in all years before 2010 (Figure S1). Many dimeric natural products deliver a broader spectrum of biological activities than their corresponding monomeric counterparts especially when target proteins rely on the formation of dimeric species for activity.[4–6] The ability to simultaneously bind two separate monomers of a dimeric receptor could potentially increase potency and efficacy or lead to the activation of cell-signaling pathways. Thus, dimerization has been increasingly adopted as a useful medicinal chemistry strategy to enhance the therapeutical potential of natural or synthetic molecules.[4–7]

The E3 ubiquitin–protein ligase, Casitas B-lineage lymphoma proto-oncogene-b (CBL-B), plays a crucial role in the regulation of both innate and adaptive immunity.[8,9] CBL-B suppresses the antitumor activities of both T cells and NK cells by negatively regulating their cellular signaling pathways.[10,11] Genetic ablation of CBL-B in mice demonstrated that the deprivation of CBL-B catalytic activity provided protection against both transplanted and spontaneous tumors.[12] Thus, CBL-B represents an attractive target for immunotherapeutic intervention in cancer. A previously established high-throughput assay was used to screen a library of >175,000 natural product fractions for inhibitors of CBL-B catalytic activity.[13,14] Bioassay-guided subfractionation of the active fractions of the marine sponge *Plakortis* sp. revealed a new dimeric alkaloid plakoramine A (**1**) (Figure 1) that potently inhibited the CBL-B catalytic activity. Plakoramine A (**1**) represents the first reported dimer of the plakinidine class of alkaloids.[15–18] Further mechanistic studies revealed an efficient self-sensitized photodimerization process for the monomeric counterpart plakinidine B (**2**) (Figure 1). The structure elucidation, CBL-B inhibitory activity, and photochemical synthesis of plakoramine A (**1**) are described in this report.

Plakoramine A (**1**) was isolated as a red solid from the organic extract of a *Plakortis* sponge which was collected in Tonga. The molecular formula of **1** was determined as $C_{38}H_{31}N_8O_3$ given the positively charged ion at *m*/*z* 647.2510 (calcd for $C_{38}H_{31}N_8O_3^+$, *m*/*z* 647.2514) detected in its HRESIMS spectrum. The ^{1}H NMR spectroscopic data (Table S1) displayed three NH protons (δ_H 10.62, 10.37, and 10.29), the coupled spin systems of two ortho-disubstituted benzenes (δ_H 9.05/8.14/8.20/8.43 and 8.15/7.41/6.74/6.30), four *N*-methyls (δ_H 3.95, 3.89, 3.39, and 3.35), and four methylenes (δ_H 3.74/3.64, 2.52/2.39, 3.75, and 2.56). The ^{13}C NMR data (Table S1) exhibited 31 out of 38 carbons in the downfield region (δ_C 102–188), indicating a high degree of aromaticity. In comparison with plakinidine B (**2**), the major metabolite of the producing *Plakortis* sponge, half of the ^{1}H and ^{13}C NMR resonances (Table S1) of **1** were nearly identical to the 1D NMR data of **2**[17] except for the methine at position 2 (δ_H 8.76, δ_C 126.2) which was replaced by a quaternary carbon in **1** (δ_C 139.5). Further analysis of the 2D NMR [^{1}H–^{1}H COSY, HMBC (pulse sequences optimized for $^nJ_{CH}$ 8 and 2 Hz), and ROESY] data (Figure 2, Table S1) confirmed that the substructure A of **1** was identical to the structure of **2** while the substituent on C-2 (substructure B) shared a similar conjugated ring system to that of substructure A. Significant changes in substructure B were observed for C-2′ (δ_C 168.6) and C-12a′ (δ_C 70.3) which were substituted for an amide carbonyl and a sp^3 quaternary carbon, respectively, from two sp^2 quaternary carbons in substructure A. Moreover, the sp^2 quaternary C-12′ resonance shifted downfield significantly from δ_C 153.6 to δ_C 174.8 indicating the presence of an exocyclic C═N double bond. The aforementioned structural modifications in substructure B were supported by the HMBC (pulse sequences optimized for $^nJ_{CH}$ 8 Hz) correlations from NH-1′ (δ_H 10.37) to C-2′, C-2a′, C-12a′, and C-12b′ and from CH$_3$-14′ (δ_H 3.39) to C-12′. The 13′-12′-11a′-7b′-8′ ensemble can be viewed as an N-8′ protonated (δ_H 10.62) resonance structure with a cation delocalizing between N-13′ and N-8′. The structural assignment was further secured by the long-range HMBC (pulse sequences optimized for $^nJ_{CH}$ 2 Hz) correlations from NH-1′ to C-2b′, C-7a′, and CH$_3$-15′, from CH$_3$-15′ (δ_H 3.95) to C-12a′ and C-12b′, and from CH$_3$-14′ to C-11′ and C-11a′. Finally, the structural elucidation of **1** was completed by connecting substructures A and B through a single bond between C-2 and C-12a′, which was supported by the long-range HMBC correlations from NH-1′ and CH$_3$-15′ to C-2.

To determine the absolute configuration of C-12′, the chiroptical properties of **1** were measured with optical polarimetry and electronic circular dichroism (ECD) spectroscopy. Compound **1** showed no optical rotation ($[\alpha]_D = 0$) or Cotton effect in its ECD spectrum (Figure S2) indicating it as a racemic mixture [(±)-**1**]. Chiral-phase HPLC separation of (±)-**1** (Figure S3) on a Lux 5 μm i-Amylose-3 column led to the optically pure enantiomers (+)-**1** ($[\alpha]^{20}_D$ 340) and (−)-**1** ($[\alpha]^{20}_D$ –335). The absolute configurations of the purified enantiomers were determined by comparison of their experimental ECD spectra with the computationally calculated spectrum of the 12a′*S* isomer (Figure 3). A conformational search was carried out using the GMMX methodology with an energy cutoff of 3 kcal/mol. Lowest energy conformers were optimized with Gaussian ‘16 using the B3LYP/DGDZVP method with the COSMO solvation model. Following TDDFT calculation at the same levels on six optimized conformers led to the simulated ECD spectrum of the 12a′*S* isomer. The ECD spectrum of (+)-**1** displayed a strong negative Cotton effect at ca. 263 nm and an

intense positive Cotton effect at ca. 352 nm which were consistent with the calculated ECD data for the 12a′*S* isomer (Figure 3). The ECD spectrum of (−)-**1** displayed Cotton effects of equal magnitude but opposite sign to those of the 12a′*S* isomer. Thus, the absolute configurations of (+)-**1** and (−)-**1** were determined as 12a′*S* and 12a′*R*, respectively (Figure 3).

The activities of (+)-**1** and (−)-**1** against the E3 ubiquitin-protein ligase CBL-B were evaluated in a biochemical assay as previously described.[13] Both (+)-**1** and (−)-**1** inhibited CBL-B activity with IC_{50} values of 7.5 and 9.7 μM, respectively (Figure 4). In contrast, the monomeric precursor **2** showed ~20 fold less potency (IC_{50} 167 μM) against CBL-B than its dimeric counterparts. It is also noteworthy that the monomer **2** showed potent antiproliferative activities (average GI_{50} 0.18 μM) (Figures S5 and S6) in the NCI-60 cell lines screen,[19] while neither (+)-**1** or (−)-**1** affected cell growth or viabilities even at high micromolar concentrations (average $GI_{50}s$ > 30 μM, Figures S7 and S8). It is known that CBL-B dimerization is required for its ubiquitin ligase activities.[20] The activation of CBL-B relies on the two critical interaction surfaces of the dimerized CBL-B ubiquitin-associated (UBA) domain which is activated by ubiquitin binding.[20] Thus, it will be interesting to further study the mechanism of plakoramine A [(±)-**1**] by investigating the importance of its dimeric architecture for its interaction with CBL-B and regulation of CBL-B activities.

In light of the racemic nature of plakoramine A [(±)-**1**], it is reasonable to hypothesize that the dimeric structure of (±)-**1** was derived from a nonenzymatic process. It was found that a trace amount of (±)-**1** was constantly detected in preparative HPLC fractions that contained mainly **2**, which provided the starting conditions for testing our hypothesis. First, a pure sample of **2** was stirred in a common HPLC solvent system [MeCN/H_2O (1:1)] at room temperature in the dark overnight, but the starting material was unchanged (Figure S9B). Further attempts to scrutinize the reaction conditions revealed that (±)-**1** was readily formed through the spontaneous dimerization of **2** in MeCN/H_2O (1:1) under both UV (Figure S9C) and white light (Figure 5A) irradiations. In contrast, the reaction of **2** in anhydrous MeCN did not provide readily detectable (±)-**1** with either UV or white light irradiations (Figure S9D) suggesting both light and solvent have a dramatic effect on conversion efficiency. Manipulation of the irradiation parameters (i.e., light source, irradiation distance, and exposure period) afforded the optimized yield of (±)-**1** at ~30% with white light irradiation of **2** in MeCN/H_2O (1:1) for 4 h using a 15 W LED (Figure 5A). Interestingly, reaction of **2** in N_2-sparged solvents led to a significant decrease of the yield of (±)-**1** from ~30% to only ~9% (Figure 5A). In total, the data suggested that the dimerization of **2** was likely driven by a photooxidative process that was catalyzed by certain reactive oxygen species (ROS) generated through the photoactivation of molecular oxygen in the aqueous environment.

To address the responsible ROS, the reactivity of **2** was tested under dark conditions with hydrogen peroxide (H_2O_2) and chemically generated singlet oxygen ($^1O_2$), hydroxyl radical ($OH^{\bullet}$), and superoxide anion ($O2^{\bullet-}$). The results clearly showed that (±)-**1** was efficiently and exclusively formed in the presence of thermally generated singlet oxygen ($^1O_2$) (Figures 5B and S10). The highly reactive singlet oxygen ($^1O_2$) is normally produced by irradiation of molecule oxygen ($^3O_2$) in the presence of a photosensitizer, such as rose

bengal, methylene blue, or porphyrins.[21] The Abs/Em spectra (Figure 5C) indicated **2** was moderately fluorescent and probably functioned as a photosensitizer. The hypothesis was tested by irradiating **2** in MeCN/H_2O (1:1) with the presence of the singlet oxygen probe 9,10-anthracenediyl-bis(methylene)-dimalonic acid (ABDA) which can be specifically oxidized to its endoperoxide analog by singlet oxygen ($^1O_2$).[22] After 2 h irradiation with white light, ABDA was completely consumed and partially converted to two γ-lactone derivatives **4** and **5** (Figure 5D and S11). It is reasonable to hypothesize that **4** and **5** were formed through a similar anthracene endoperoxide degradation pathway as previously described[23] with the participation of a key zwitterion intermediate **a** (Figure S12). Finally, the **2**-sensitized photosynthesis of singlet oxygen ($^1O_2$) was confirmed by indirect detection and quantification of $^1O_2$ by electron paramagnetic resonance (EPR) using a $^1O_2$-specific spin trap 2,2,6,6-tetramethyl-4-piperidone (4-Oxo-TEMP).[24] Singlet oxygen ($^1O_2$) was steadily generated in a time-dependent manner with continuous white light irradiation. The production of $^1O_2$ reached its near-to-maximal yield after around 4 h (Figure 5E) showing good agreement with the kinetics of (±)-**1** formation (Figure 5A).

Based on the aforementioned evidence, a plausible mechanism was proposed for the photochemical dimerization of **2** (Scheme 1). First, aqueous conditions may facilitate formation of the zwitterionic resonance form of **2**. Upon light irradiation, the triplet excited state of **2** sensitizes molecular oxygen ($^3O_2$) to form the reactive singlet oxygen ($^1O_2$) which directly attacks the pyrrole moiety of the zwitterion form via [4 + 2] cycloaddition to yield the endoperoxide intermediate **a**.[25–27] Well-precedented ring opening of the endoperoxide reveals an electrophilic iminium ion **b**, which is then subject to nucleophilic attack by C-2 of another molecule of **2** to form the C-12a′/C-2 bridge. Final hydroperoxide decomposition forms the γ-lactam product (±)-**1**.

Plakoramine A [(±)-**1**] represents the first example of a novel class of heterodimeric alkaloids that provides a promising pharmacophore for chemical intervention of the anticancer target E3 ubiquitin-protein ligase CBL-B. The naturally occurring, monomeric counterpart plakinidine B (**2**) also stands for a new functional fluorophore with potential utility as both a photosensitizer and a photochemically triggered electrophilic agent.

Supplementary Material

Refer to Web version on PubMed Central for supplementary material.

Acknowledgments

We thank the Natural Products Support Group (NCI at Frederick) for the extract preparation and Emily Smith (Basic Science Program, Leidos Biomedical Research, Inc., Frederick National Laboratory for Cancer Research) for CBL-B assay support. We also thank Lauren Procter, Morgan Pagonis, and Jane Jones of the FNLCR Protein Expression Laboratory for their recombinant protein production efforts.

REFERENCES

(1). Snyder SA Organic chemistry: symmetrizing the unsymmetrical. Nature 2010, 465, 560–561. [PubMed: 20520702]

(2). Liu J; Liu A; Hu Y Enzymatic dimerization in the biosynthetic pathway of microbial natural products. Nat. Prod. Rep. 2021, 38, 1469–1505. [PubMed: 33404031]

(3). Voloshchuk T; Farina NS; Wauchope OR; Kiprowska M; Haberfield P; Greer A Molecular bilateral symmetry of natural products: prediction of selectivity of dimeric molecules by density functional theory and semiempirical calculations. J. Nat. Prod. 2004, 67, 1141–1146. [PubMed: 15270568]

(4). Berube G Natural and synthetic biologically active dimeric molecules: anticancer agents, anti-HIV agents, steroid derivatives and opioid antagonists. Curr. Med. Chem. 2006, 13, 131–154. [PubMed: 16472210]

(5). Paquin A; Reyes-Moreno C; Berube G Recent advances in the use of the dimerization strategy as a means to increase the biological potential of natural or synthetic molecules. Molecules 2021, 26, 2340. [PubMed: 33920597]

(6). Hadden MK; Blagg BS Dimeric approaches to anti-cancer chemotherapeutics. Anticancer Agents Med. Chem. 2008, 8, 807–816. [PubMed: 18855582]

(7). Sun J; Yang H; Tang W Recent advances in total syntheses of complex dimeric natural products. Chem. Soc. Rev. 2021, 50, 2320–2336. [PubMed: 33470268]

(8). Bhoj VG; Chen ZJ Ubiquitylation in innate and adaptive immunity. Nature 2009, 458, 430–437. [PubMed: 19325622]

(9). Liu YC Ubiquitin ligases and the immune response. Annu. Rev. Immunol. 2004, 22, 81–127. [PubMed: 15032575]

(10). Liyasova MS; Ma K; Lipkowitz S Molecular pathways: Cbl proteins in tumorigenesis and antitumor immunity-opportunities for cancer treatment. Clin. Cancer Res. 2015, 21, 1789–1794. [PubMed: 25477533]

(11). Paolino M; Choidas A; Wallner S; Pranjic B; Uribesalgo I; Loeser S; Jamieson AM; Langdon WY; Ikeda F; Fededa JP; Cronin SJ; Nitsch R; Schultz-Fademrecht C; Eickhoff J; Menninger S; Unger A; Torka R; Gruber T; Hinterleitner R; Baier G; Wolf D; Ullrich A; Klebl BM; Penninger JM The E3 ligase Cbl-b and TAM receptors regulate cancer metastasis via natural killer cells. Nature 2014, 507, 508–512. [PubMed: 24553136]

(12). Chiang JY; Jang IK; Hodes R; Gu H Ablation of Cbl-b provides protection against transplanted and spontaneous tumors. J. Clin. Invest. 2007, 117, 1029–1036. [PubMed: 17364027]

(13). Wilson BAP; Voeller D; Smith EA; Wamiru A; Goncharova EI; Liu G; Lipkowitz S; O'Keefe BR In Vitro Ubiquitination Platform Identifies Methyl Ellipticiniums as Ubiquitin Ligase Inhibitors. SLAS Discovery 2021, 26, 870–884. [PubMed: 33882749]

(14). Wilson BAP; Thornburg CC; Henrich CJ; Grkovic T; O'Keefe BR Creating and screening natural product libraries. Nat. Prod. Rep. 2020, 37, 893–918. [PubMed: 32186299]

(15). Ford PW; Davidson BS Plakinidine D, a new pyrroloacridine alkaloid from the ascidian *Didemnum rubeum*. J. Nat. Prod. 1997, 60, 1051–1053. [PubMed: 9358649]

(16). Smith CJ; Venables DA; Hopmann C; Salomon CE; Jompa J; Tahir A; Faulkner DJ; Ireland CM Plakinidine D, a new pyrroloacridine alkaloid from two ascidians of the genus *Didemnum*. J. Nat. Prod. 1997, 60, 1048–1050. [PubMed: 9358648]

(17). West RR; Mayne CL; Ireland CM; Brinen LS; Clardy J Plakinidines: Cytotoxic alkaloid pigments from the Fijian sponge *Plakortis* sp. Tetrahedron Lett. 1990, 31, 3271–3274.

(18). Inman WD; Oneilljohnson M; Crews P Novel Marine Sponge Alkaloids. 1. Plakinidine A and B, anthelmintic active alkaloids from a *Plakortis* sponge. J. Am. Chem. Soc. 1990, 112, 1–4.

(19). Shoemaker RH The NCI60 human tumour cell line anticancer drug screen. Nat. Rev. Cancer 2006, 6, 813–823. [PubMed: 16990858]

(20). Peschard P; Kozlov G; Lin T; Mirza IA; Berghuis AM; Lipkowitz S; Park M; Gehring K Structural basis for ubiquitin-mediated dimerization and activation of the ubiquitin protein ligase Cbl-b. Mol. Cell 2007, 27, 474–485. [PubMed: 17679095]

(21). Greer A Christopher Foote's discovery of the role of singlet oxygen [1O2 ($^1\Delta_g$)] in photosensitized oxidation reactions. Acc. Chem. Res. 2006, 39, 797–804. [PubMed: 17115719]

(22). Entradas T; Waldron S; Volk M The detection sensitivity of commonly used singlet oxygen probes in aqueous environments. J. Photochem. Photobiol., B 2020, 204, 111787. [PubMed: 31958676]

(23). Mao X; Zhang J; Wang X; Zhang H; Wei P; Sung HHY; Williams ID; Feng X; Ni XL; Redshaw C; Elsegood MRJ; Lam JWY; Tang BZ An air-stable organic radical from a controllable photoinduced domino reaction of a hexa-aryl substituted anthracene. J. Org. Chem. 2021, 86, 7359–7369. [PubMed: 34032439]

(24). Lin Y; Yang Q; Geng F; Feng H; Chen M; Hu B Suppressing singlet oxygen formation during the charge process of Li-O2 batteries with a Co_3O_4 solid catalyst revealed by operando electron paramagnetic resonance. J. Phys. Chem. Lett 2021, 12, 10346–10352. [PubMed: 34665633]

(25). Lightner DA; Bisacchi GS; Norris RD On the mechanism of the sensitized photooxygenation of pyrroles. J. Am. Chem. Soc. 1976, 98, 802–807.

(26). Alberti MN; Vougioukalakis GC; Orfanopoulos M Photosensitized oxidations of substituted pyrroles: unanticipated radical-derived oxygenated products. J. Org. Chem. 2009, 74, 7274–7282. [PubMed: 19739608]

(27). Howard JK; Rihak KJ; Bissember AC; Smith JA The oxidation of pyrrole. Chem.—Asian J 2016, 11, 155–167. [PubMed: 26294175]

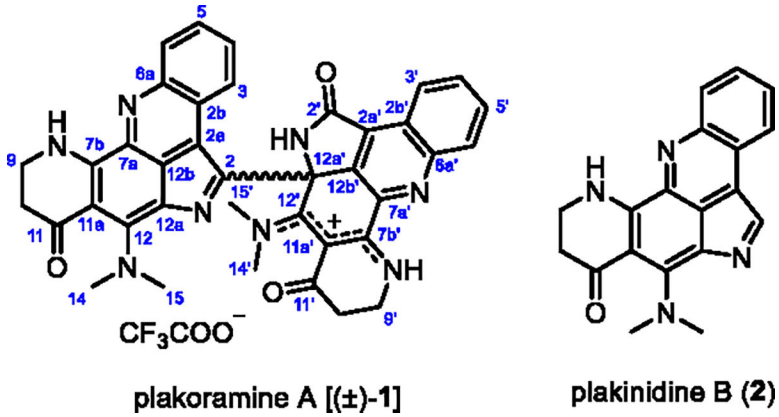

Figure 1.
Structures of compounds (±)-**1** and **2**.

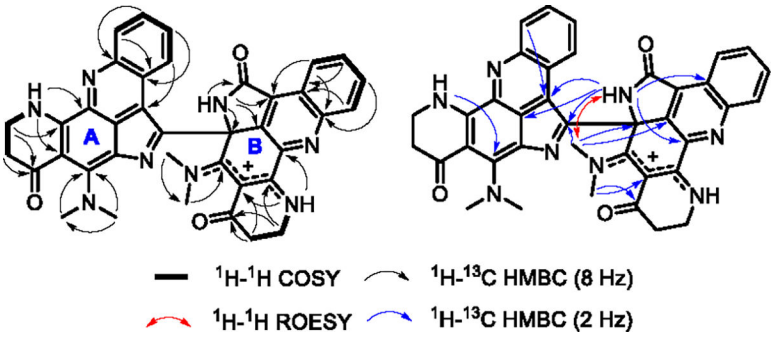

Figure 2.
Selected 2D NMR correlations of compound (±)-**1**.

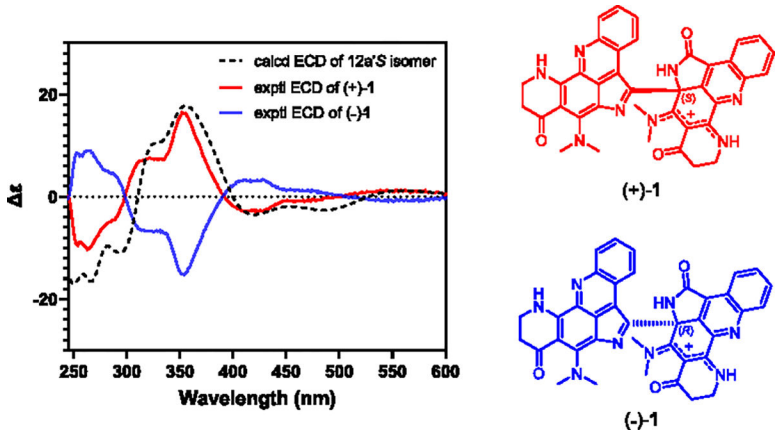

Figure 3.

Comparison of the experimental ECD spectra of (+)-**1** and (−)-**1** with the calculated ECD spectrum of the 12a′*S* isomer of (±)-**1**.

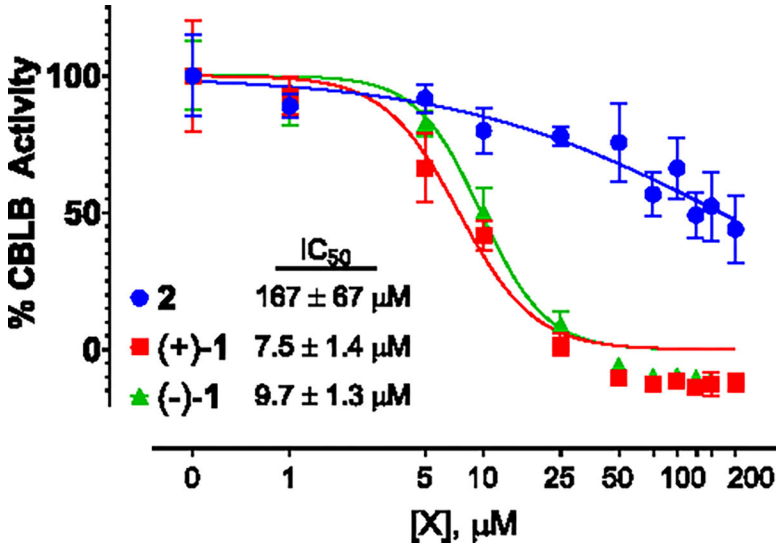

Figure 4.

Dose–response curves of **2**, (+)-**1**, and (−)-**1** in the CBL-B biochemical assay.

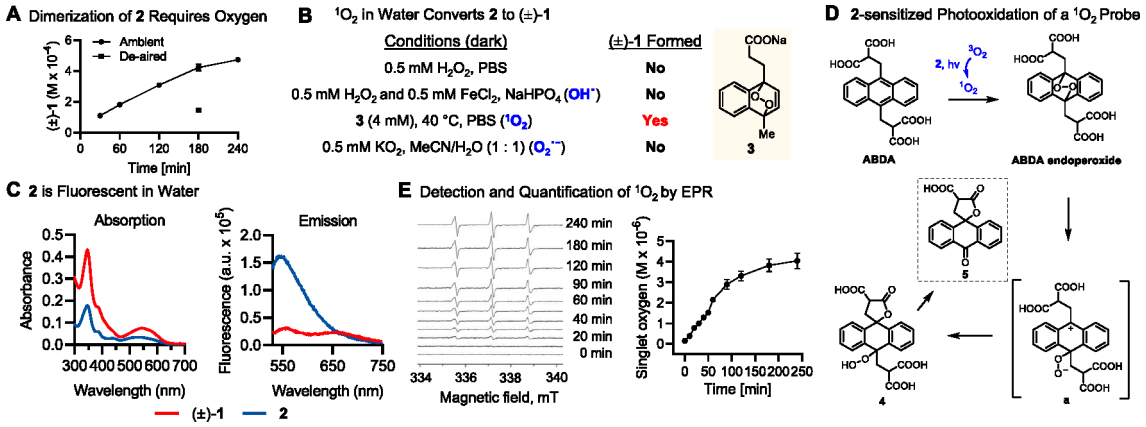

Figure 5.

Mechanistic studies of the photochemical dimerization of **2**. (A) Time-dependent production of (±)-**1** was monitored by HPLC-PDA following irradiation of **2** (1 mg/mL) in 1:1 MeCN/H_2O with white light (15 W, LED) for 4 h under ambient and deaired conditions. (B) Evaluating the dimerization of **2** to (±)-**1** with independently generated ROS under dark conditions. (C) UV–vis absorption and fluorescence emission (520 nm excitation) spectra of **2** and (±)-**1**. (D) Plakinidine B (**2**)-sensitized photooxidation of the $^1O_2$ probe ABDA. (E) Detection and quantification of $^1O_2$ by electron paramagnetic resonance (EPR) using spin traps and the 4-Oxo-TEMP redox probe. Time-dependent production of $^1O_2$ was monitored following irradiation of **2** (1 mg/mL) in 1:1 MeCN/H_2O with white light for 4 h under ambient conditions. All quantitative values were obtained from three independent experiments and graphed as mean ± SEM.

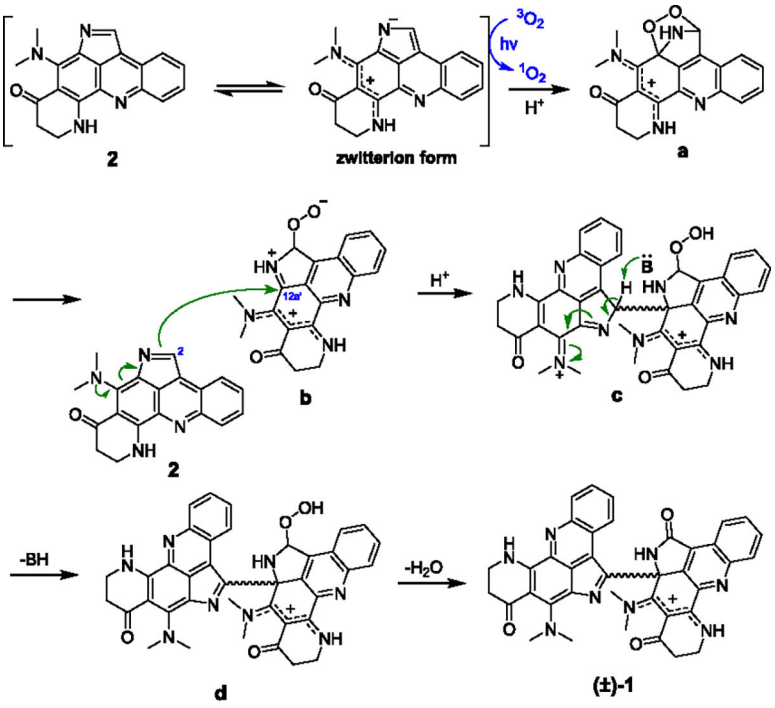

Scheme 1.
Proposed Mechanism of the Photochemical Dimerization of 2